Prediction of Li intercalation voltages in rechargeable battery cathode materials: Effects of exchange-correlation functional, van der Waals interactions, and Hubbard *U*

Eric B. Isaacs, Shane Patel, and Chris Wolverton*
Department of Materials Science and Engineering, Northwestern University, Evanston, Illinois 60208, USA

(Received 5 March 2020; accepted 3 June 2020; published 18 June 2020)

Quantitative predictions of the Li intercalation voltage and of the electronic properties of rechargeable battery cathode materials are a substantial challenge for first-principles theory due to the possibility of (1) strong correlations associated with localized transition metal *d* electrons and (2) significant van der Waals (vdW) interactions in layered systems, both of which are not accurately captured by standard approximations to density functional theory (DFT). Here, we perform a systematic benchmark of electronic structure methods based on the widely used generalized-gradient approximation of Perdew, Burke, and Ernzerhof (PBE) and the new strongly constrained and appropriately normed (SCAN) meta-generalized-gradient approximation for battery cathode materials. Studying layered Li_xTiS_2, Li_xNiO_2, and Li_xCoO_2, olivine Li_xFePO_4, and spinel $Li_xMn_2O_4$, we compute the voltage, crystal structure, and electronic structure with and without extensions to incorporate onsite Hubbard interactions and vdW interactions. Within pure DFT (i.e., without corrections for onsite Hubbard interactions), SCAN is a significant improvement over PBE for describing cathode materials, decreasing the mean absolute voltage error by more than 50%. Although explicit vdW interactions are not critical and in cases even detrimental when applied in conjunction with SCAN, Hubbard-*U* corrections are still in general necessary to achieve reasonable agreement with experiment. We show that no single method considered here can accurately describe the voltage and overall structural, electronic, and magnetic properties (i.e., errors no more than 5% for voltage, volume, band gap, and magnetic moments) of battery cathode materials, motivating a strong need for improved electronic structure approaches for such systems.

DOI: 10.1103/PhysRevMaterials.4.065405

I. INTRODUCTION

Li-ion rechargeable battery cathodes, which are typically composed of transition metal oxides, represent a challenging test bed for first-principles theory. Prediction of the Li intercalation voltage is of particular importance given it is a fundamental battery property that helps determine the battery power and closely relates to the (de)lithiation mechanism. The average Li intercalation voltage V corresponds to the difference in Li chemical potential between the cathode and anode. As discussed in detail in Refs. [1,2], for a battery cathode whose Li content varies between x_1 to $x_2 > x_1$, the average voltage V relative to Li metal is given by $eV = E_{\mathrm{Li}} + \frac{E(x_1)-E(x_2)}{(x_2-x_1)}$, where e is the elementary charge, E_{Li} is the energy of Li metal, $E(x)$ is the energy of the cathode material with Li concentration x, and it is assumed all the displaced charge is due to Li. For example, for Li_xCoO_2, over the full crystallographic range of Li ($x_1 = 0$ for CoO_2, $x_2 = 1$ for $LiCoO_2$), V is given by $eV = E_{\mathrm{Li}} + E(0) - E(1)$. In principle, Gibbs free energies should be used in the previous expressions; we ignore pressure-volume and entropic contributions typically small compared to the magnitude of V [3]. Since V is a function of the total energies of phases whose electron distributions differ starkly (leading to fewer opportunities for error cancellation), it is a useful observable to serve as a stringent benchmark of *ab initio* thermodynamics approaches.

Density functional theory (DFT) [4,5], within the generalized-gradient approximation (GGA) [6] in particular, has become a very widely used method for electronic structure calculations of solids. Despite its many successes, DFT struggles to capture the composition-dependent energetics necessary to describe the intercalation voltage and compositional phase stability of battery cathode materials. For example, in the case of olivine Li_xFePO_4 [7,8], DFT in the GGA substantially underestimates the experimental V (by ∼20%) and fails to qualitatively capture the experimentally observed phase separation for intermediate Li concentrations [9,10]. In order to address this challenge, a wide variety of electronic structure approaches, including DFT with different exchange-correlation functionals [1,2,11–13], hybrid functionals [14,15], van der Waals (vdW) functionals [16], DFT plus onsite Hubbard U (DFT + U) [10,17–21], DFT + U + V (where V is an intersite interaction) [22], DFT plus dynamical mean-field theory [23], and diffusion quantum Monte Carlo [24] have been applied to battery cathode voltages. It remains an open question as to what interactions and level of theory beyond DFT in the GGA are needed to adequately describe such materials.

Among these works, we mention two recent developments pertaining to cathode voltage prediction. The first is the work of Aykol *et al.*, who found that vdW interactions, employed in conjunction with DFT + U and the widely used GGA of

*c-wolverton@northwestern.edu

Perdew, Burke, and Ernzerhof (PBE), are necessary to accurately describe the voltage for layered Li_xCoO_2 [16]. Second, also studying layered cathode materials, Chakraborty *et al.* found that the new strongly constrained and appropriately normed (SCAN) DFT functional considerably improves the voltage prediction even without Hubbard-U or explicit vdW corrections [13].

In this work, we perform a systematic study of the average Li intercalation voltage of five classic cathode materials: layered Li_xTiS_2, olivine Li_xFePO_4, layered Li_xNiO_2, spinel $Li_xMn_2O_4$, and layered Li_xCoO_2. For the five cathode materials, we investigate the impact on V of (1) the new SCAN exchange-correlation functional, (2) the use of density functionals explicitly considering vdW interactions, and (3) onsite Hubbard U within DFT + U, whereas past studies have mainly focused on DFT + U based solely on PBE and/or restricted attention to a single class of cathodes. In all cases, our calculations are critically compared to experiments to assess accuracy. We also consider other quantities (volumes, electronic band gaps, and magnetic moments) in order to provide a more complete picture of the accuracy of the methods.

Within pure DFT,[1] we find that SCAN is a significant improvement for describing battery cathode materials, decreasing the mean absolute error for V by more than 50%, as compared to PBE [6], from 0.67 to 0.30 V. In some cases (e.g., Li_xFePO_4 and $Li_xMn_2O_4$) Hubbard-U corrections are still necessary to achieve reasonable agreement (i.e., within 5%) with experiment. Therefore, given the improvement of SCAN over PBE, quantitative voltage predictions within pure DFT are closer but still currently out of reach. When applied in combination with SCAN, Hubbard U within DFT + U can lead to worsened predictions in some cases (i.e., Li_xTiS_2 and Li_xCoO_2). In other words, within DFT + U, Hubbard U added to SCAN does not universally help or hurt the predictions. In the one case in which SCAN itself provides a sufficient prediction of V (i.e., Li_xNiO_2), we find it is still possible to achieve a better overall electronic structure description using DFT + U calculations based on PBE rather than SCAN. Therefore, calculations based on SCAN should not necessarily be considered universally better than those based on PBE when considering both the energetics and overall electronic structure. Using PBE, adding vdW interactions provides appreciably improved V predictions, even for nonlayered cathode materials lacking a clear van der Waals gap when delithiated. In the majority of the cases, when Hubbard U is also considered with PBE, the experimental V can be achieved with or without vdW interactions (for different values of U). Therefore, it is not clear that missing vdW interactions are a significant source of PBE's well-known voltage underprediction in general. We find that such vdW interactions are significantly less important in terms of V when applied in conjunction with SCAN, which already contains some intermediate-range vdW interactions. Overall, despite the significantly improved V predictions of SCAN as compared to PBE within pure DFT, we illustrate that no single method considered here can generally describe the voltage and overall electronic structure of battery cathode materials, motivating a strong need for improved electronic structure approaches for such systems.

[1]We use "pure DFT" to refer to all the methodologies studied in this work without Hubbard-U corrections, such that the total energy is purely a functional of the density (even if only implicitly). This includes SCAN and the vdW functionals.

II. SUMMARY OF ELECTRONIC STRUCTURE APPROACHES TESTED

A. Exchange-correlation functional

The key ingredient to DFT is the exchange-correlation functional E_{xc}, which encapsulates all the interaction effects beyond the single-particle kinetic energy and mean-field (Hartree) Coulomb energy [25]. E_{xc} in the local density approximation (LDA) depends solely on the electron density ρ and is parametrized to exactly describe the homogeneous electron gas (jellium) [26]. In GGA, E_{xc} depends on $\nabla\rho$ in addition to ρ, which allows for the satisfaction of additional constraints such as the correct behavior in the slowly and rapidly varying density limits [6]. A higher level of theory is the meta-GGA, in which E_{xc} exhibits an additional dependence on the orbital kinetic energy density

$$\tau = \sum_i \frac{1}{2}|\nabla\psi_i|^2, \tag{1}$$

where ψ_i is the ith occupied Kohn-Sham wave function, corresponding to functional that is implicitly nonlocal in ρ.

The strongly constrained and appropriately normed (SCAN) functional [27] is a new meta-GGA, which satisfies 17 known constraints of the exact E_{xc} and has shown significant promise in the description of solids [27–31]. Just as PBE is built on top of LDA (reproducing the LDA result for jellium), SCAN is built on top of PBE and exhibits the same behavior as PBE for slowly varying densities in the metallic bonding regime of τ. Due to its nonlocality in ρ and the consideration of systems with nonbonded interactions in its construction, the SCAN functional implicitly contains some "intermediate-range" vdW interactions [27]. It also can be incorporated in methods containing explicit vdW interactions [32], as discussed below. Although SCAN is not explicitly constructed to capture strong electronic correlations, it has been recently applied to correlated materials such as the cuprate La_2CuO_4 [33]. We note that SCAN has been shown to exhibit more numerical convergence issues compared to PBE [34–36].

Very relevant to the prediction of battery cathode voltages is that SCAN has been shown to yield significant improvement to formation energy predictions as compared to PBE for strongly bound compounds like oxides [37,38]. Indeed, for a few layered cathode materials, very recent work has suggested that SCAN achieves more accurate V prediction compared to PBE [13,23]. In particular, based on calculations of layered Li_xNiO_2, Li_xCoO_2, and Li_xMnO_2 with PBE, PBE + U, and SCAN, Chakraborty *et al.* found that SCAN performs better than PBE and PBE + U for the V profiles. Based on the V behavior, as well as predicted lattice parameters, densities of states, and ρ (as compared to that from the PBE0 hybrid functional), they concluded that SCAN without Hubbard U exhibits good overall performance for layered cathode

materials. Whether such trends hold more generally (e.g., for nonlayered cathodes) is an open question addressed by this work.

B. Explicit van der Waals interactions

The lack of nonlocal correlation effects needed to capture vdW interactions is a well-documented limitation of standard DFT [39–44]. In order to address this limitation, first-principles vdW density functionals have been developed. In such functionals, a nonlocal correlation energy term (explicitly nonlocal in ρ) of the form

$$E_c^{nl} = \frac{1}{2}\iint \rho(r)\phi(r,r')\rho(r')d^3r\,d^3r' \tag{2}$$

is incorporated in E_{xc} [45,46]. Here, $\phi(r,r')$ is the kernel, which is typically based on approximations to the frequency-dependent polarizability. For example, Dion *et al.* devised a kernel based on a plasmon pole approximation to the dielectric function ϵ and a second-order expansion of the polarization $S = 1 - \epsilon^{-1}$ [42,45], such that the kernel is a function of ρ and $\nabla\rho$ at spatial coordinates r and r' as well as $|r - r'|$.

Aykol *et al.* recently tested a variety of methodologies incorporating vdW interactions (including first-principles and semiempirical approaches) on Li_xCoO_2 [16]. The first-principles opt-type vdW density functionals [47,48], such as optPBE-vdW, were found to yield the most accurate V predictions and correspond to a significant improvement over standard density functionals lacking vdW interactions. This opens up the question of how important vdW interactions are to describe battery cathode materials in general (i.e., beyond Li_xCoO_2), which we address in this work.

We focus on optPBE-vdW in this work [47,48]. optPBE-vdW combines a linear combination of the exchange forms of PBE and the related RPBE [49], LDA local correlation, and the kernel of Ref. [45]. In optPBE-vdW, the fraction of PBE-like [6] and RPBE-like [49] exchange and the two parameters employed in both such forms have been optimized (hence the "opt") to minimize interaction energy errors for the Set 22 (S22) quantum chemistry benchmark [50]. When we refer to adding vdW interactions to PBE in this work, we are referring to the optPBE-vdW method. Although this is not strictly accurate as the difference between PBE and optPBE-vdW is not additive, we do so for convenience and since optPBE-vdW is closely connected to PBE. We also consider the SCAN plus revised Vydrov–Van Voorhis 2010 (SCAN+rVV10) vdW functional [32,51,52], which corresponds to a different choice of kernel with one of its two parameters fit to best reproduce the Ar dimer binding curve from coupled-cluster singles, doubles, and perturbative triples [CCSD(T)] quantum chemistry calculations. SCAN+rVV10 is explored in this work for purely practical reasons as it is currently the only vdW functional implemented in conjunction with the SCAN functional in the Vienna *ab initio* simulation package (VASP). In this work, we also refer to SCAN+rVV10 as SCAN+vdW for convenience.

C. Onsite Hubbard-U corrections

In an attempt to correct for the deficiencies of DFT (using common approximations like the GGA), the DFT + U approach [53] has become a widely used method to describe cathode materials. In this methodology, DFT is augmented with an onsite Hubbard interaction U (solved within static mean-field theory) related to strong electronic correlations in a chosen subspace of localized orbitals (defined via transition metal d-orbital projectors in this work). In this methodology, the energy depends on the onsite density matrix for the transition metal d orbitals in addition to ρ. In particular, using the simplified rotationally invariant formalism of Dudarev *et al.* [54] and the fully localized limit (FLL) double counting [55], the DFT + U energy can be written as

$$E_{\mathrm{DFT}+U} = E_{\mathrm{DFT}}[\rho^s] + \frac{1}{2}U\sum_{\tau,m,s} n_m^{\tau s}\left(1 - n_m^{\tau s}\right), \tag{3}$$

where ρ^s is the spin density, $E_{\mathrm{DFT}}[\rho^s]$ is the (spin-dependent) DFT energy, and $n_m^{\tau s}$ is the mth eigenvalue of the density matrix corresponding to transition metal site τ and spin projection s. Written this way, it is visible that the effect of DFT + U is to penalize noninteger occupancy of the localized orbitals.

DFT + U has been shown to help alleviate the voltage underestimation of DFT in the GGA [10], and it has become a standard tool to describe cathode materials. However, recent evidence suggests it may lead to considerable problems. In particular, for Li_xCoO_2, DFT + U yields spurious gaps and charge ordering, as well as overestimated Li order-disorder temperatures [21]. The ability of DFT + U to accurately describe cathode materials in general is an open question we aim to address in this work. We note that DFT + U is a static approximation to the more accurate DFT plus dynamical mean-field theory (DFT+DMFT), in which the local correlation problem is solved exactly rather than via the Hartree-Fock approximation of DFT + U. Recent DFT+DMFT calculations found a significantly different V prediction for Li_xCoO_2 as compared to DFT + U, suggesting dynamical correlations neglected by DFT + U but captured by DFT+DMFT may also be important in battery cathode materials [23]. However, due to the large computational cost to solve the quantum impurity problem in DFT+DMFT, we do not explore the role of dynamical correlations in this work.

III. COMPUTATIONAL DETAILS

Spin-dependent density functional theory calculations using the projector augmented wave (PAW) method [56,57] and a 520-eV plane-wave kinetic energy cutoff are performed using VASP [58–61]. We use the Perdew-Burke-Ernzerhof (PBE) GGA [6] and the strongly constrained and appropriately normed (SCAN) [27] meta-GGA to the exchange-correlation functional. The impact of vdW interactions is assessed via calculations with the optPBE-vdW functional [47,48] and the SCAN+rVV10 functional [32]. Onsite Hubbard U is included for the transition metal d states using the rotationally invariant DFT + U approach [53,62]. We use the recommended VASP 5.2 PBE PAW potentials for all calculations [63]. Uniform k meshes are chosen with $\geqslant 8000/N_{\mathrm{atoms}}$ k points, where N_{atoms} is the number of atoms in the unit cell. The ionic forces and total energy are converged to 10^{-2} eV/Å and 10^{-6} eV, respectively. We employ 0.1-eV first-order Methfessel-Paxton

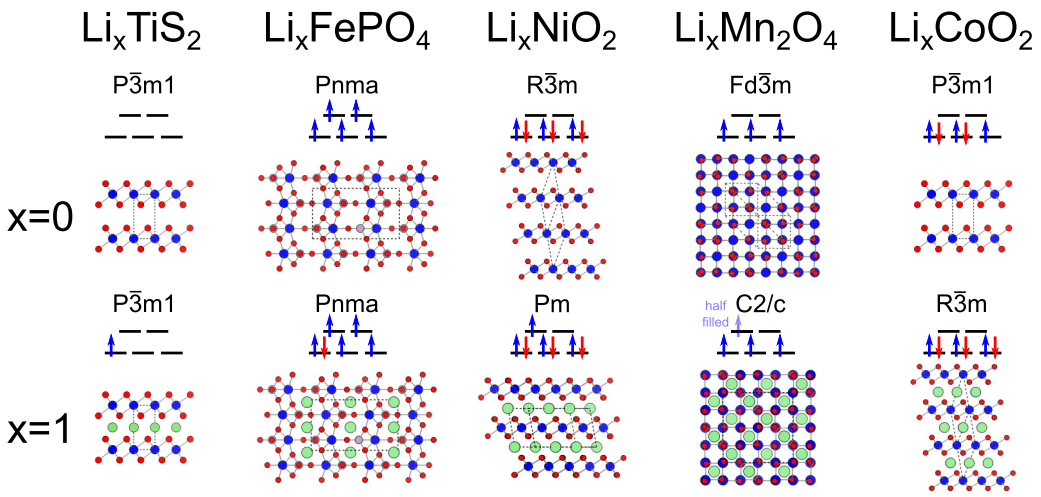

FIG. 1. Crystal structures for the fully delithiated (top, $x = 0$) and fully lithiated (bottom, $x = 1$) cathode materials studied in this work. Green, blue, red, and purple circles correspond to Li, transition metal, oxygen, and phosphorus atoms, respectively, and the unit cell is indicated by black dashed lines. Above each crystal structure, the space group and nominal transition metal d electronic configuration, assuming 1+ Li oxidation state and 2− oxidation state, are given. For simplicity, we only show the octahedral crystal-field splitting into the three lower-energy t_{2g} levels and two higher-energy e_g levels. In the case of $LiMn_2O_4$, the e_g manifold is nominally occupied by $\frac{1}{2}$ an electron per Mn on average, as indicated by the "half-filled" label.

smearing [64] for structural relaxations and the tetrahedron method with Blöchl corrections [65] for static runs.

IV. RESULTS AND DISCUSSION

A. Crystal structures and nominal electronic configurations

We begin by briefly discussing the structures and electronic configuration of the cathode materials considered. The crystal structures and nominal transition metal (TM) d-electron configurations for the five cathode materials are illustrated in Fig. 1. All the compounds considered have octahedral coordination of TM by oxygen. Although the octahedra are often distorted, we still refer to the lowest-energy three d levels as t_{2g} and the highest-energy two d levels as e_g for simplicity, where t_{2g} and e_g are the irreducible representations of d orbitals in perfect octahedral symmetry.

Li_xTiS_2, Li_xNiO_2, and Li_xCoO_2 are layered materials with alternating layers of Li and edge-sharing TM-oxygen octahedra. TiS_2 ($t_{2g}^0 e_g^0$), $LiTiS_2$ ($t_{2g}^1 e_g^0$), and CoO_2 ($t_{2g}^5 e_g^0$) are in the hexagonal $P\bar{3}m1$ structure (O1 structure) [66–68]. NiO_2 and $LiCoO_2$ (both $t_{2g}^6 e_g^0$) are considered in the rhombohedral $R\bar{3}m$ structure (O3 structure) [69–72]. We model $LiNiO_2$ ($t_{2g}^6 e_g^1$) with the monoclinic Pm structure [73], which captures the Jahn-Teller distortion. For the Li_xCoO_2 case, in addition to computing V for the full $0 < x < 1$ range, we also compute V for $x < \frac{1}{2}$ and $x > \frac{1}{2}$. To do so, we consider $Li_{1/2}CoO_2$ in the known monoclinic $P2/m$ structure, which corresponds to an in-plane Li/vacancy ordering in a unit cell twice as large as the primitive rhombohedral cell [74].

In contrast to the other materials, Li_xFePO_4 and $Li_xMn_2O_4$ do not exhibit layered crystal structures. Olivine $FePO_4$ ($t_{2g}^3 e_g^2$) and $LiFePO_4$ ($t_{2g}^4 e_g^2$) crystallize in an orthorhombic $Pnma$ structure consisting of (1) one-dimensional channels of Li and (2) layers of corner sharing Fe-oxygen octahedra connected via phosphate groups [75,76]. To model $Li_xMn_2O_4$, we consider Mn_2O_4 ($t_{2g}^3 e_g^0$) in the ideal spinel-like $Fd\bar{3}m$ structure (λ-MnO_2), which consists of a diamond sublattice of Li and a three-dimensional network of edge-sharing Mn-oxygen octahedra [77,78]. In order to capture possible Jahn-Teller effects, we model $LiMn_2O_4$ (nominally in the $t_{2g}^{3.5} e_g^0$ configuration) with the symmetry-broken ferromagnetic monoclinic $C2/c$ structure from Ref. [79]. Ferromagnetic ordering is considered for all magnetic compounds except Li_xFePO_4, which exhibits antiferromagnetic ordering [76].

B. Pure DFT

Figure 2 shows the average intercalation voltages over the full Li concentration range ($0 < x < 1$) within pure DFT ($U = 0$). The experimental values used for

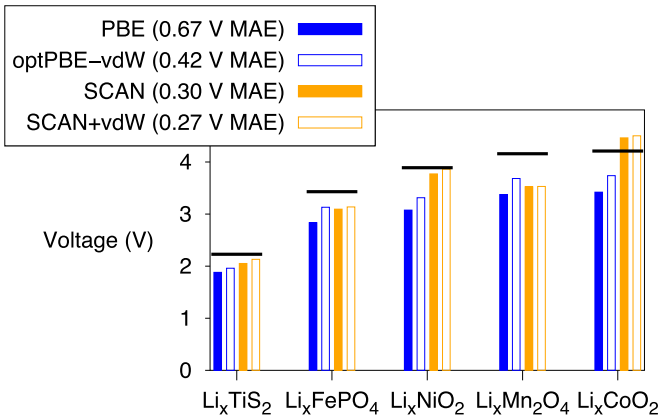

FIG. 2. Average intercalation voltage for $0 < x < 1$ within PBE, optPBE-vdW, SCAN, and SCAN+vdW for DFT (i.e., $U = 0$). The solid black horizontal lines indicate the experimental voltage. Mean absolute error (MAE) values for the five cathode materials are indicated in the legend.

Li_xTiS_2 [80], Li_xFePO_4 [8], Li_xNiO_2 [81], $Li_xMn_2O_4$ [82], and Li_xCoO_2 [68] are discussed in the Supplemental Material [83]. As has been shown previously [10], PBE systematically and substantially underpredicts V, yielding a mean absolute error (MAE) of 0.67 V. SCAN represents a significant improvement over PBE in terms of the predicted V, reducing the MAE by over 50% to 0.30 V. However, some errors are still unacceptably large (e.g., 15% error for $Li_xMn_2O_4$). In this sense, quantitative V predictions within DFT are closer to being achieved but are still currently out of reach. For most of the cathode materials, SCAN still underpredicts the experimental values despite the appreciable increase in V with respect to PBE values. There are two exceptions to this trend: (1) Li_xNiO_2, for which the SCAN prediction (3.8 V) is nearly identical to the experimental value (3.9 V) and (2) Li_xCoO_2, for which the SCAN prediction (4.5 V) is appreciably larger than experiment (4.2 V). The increase in V of SCAN with respect to PBE is highly system dependent: while this increase is 1.0 V for Li_xCoO_2, it is a mere 0.2 V for $Li_xMn_2O_4$.

Explicit vdW interactions also generally yield an increase in predicted V, though of a smaller magnitude. For example, adding vdW interactions to PBE (i.e., optPBE-vdW) reduces the MAE from 0.67 to 0.42 V. Here, the voltage increases are less system dependent: similar increases of 0.1–0.3 V (4%–10%) for optPBE-vdW with respect to PBE are found for all five cathode materials. The V enhancement is not generally smaller for nonlayered materials: V increases by 10% for Li_xFePO_4, for example. In contrast, adding vdW interactions to SCAN (i.e., SCAN+vdW) does not appreciably increase predicted V and an MAE of 0.27 V (negligibly smaller than the 0.30 V value for SCAN) is obtained. We believe this behavior stems from the construction of SCAN+vdW since a parameter in the rVV10 form is fit specifically for SCAN, which already intrinsically contains some intermediate-range vdW interactions. Based on the predicted V behavior, we find that explicit vdW methods are not critical when applied in conjunction with SCAN for battery cathode materials. This suggests that the vdW interactions intrinsic to SCAN are likely sufficient to describe vdW interactions in this class of materials. We note that Chakraborty *et al.* reached a similar conclusion using a distinct dispersion-corrected DFT approach [13].

The predicted volume is another observable with which we can benchmark different computational methods. As shown in Fig. 3, we find SCAN+vdW leads to worsened volume predictions compared to SCAN for all the systems considered. This suggests that the explicit vdW interactions contained within SCAN+vdW may be not only unnecessary, but even harmful to the description of battery cathode materials. This behavior is in contrast to that of optPBE-vdW, which generally improves the volume predictions as compared to PBE.

We note that the impact of the explicit vdW interactions on V is not primarily structural in nature. For example, freezing to PBE ground-state structures, the SCAN V value for Li_xCoO_2 changes by only 24 meV relative to the value calculated using the SCAN ground-state structures. We find similar behavior for the other cathode materials. For example, for Li_xTiS_2, the computed V changes by at most 0.1 V for the case with structures relaxed with vdW interactions and that with structures relaxed without vdW interactions, for all the functionals considered.

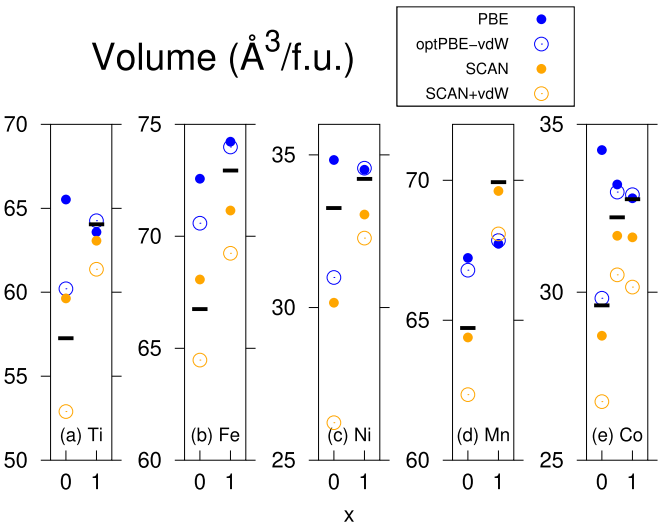

FIG. 3. Volumes in Å^3 per formula unit within pure DFT for (a) Li_xTiS_2, (b) Li_xFePO_4, (c) Li_xNiO_2, (d) $Li_xMn_2O_4$, and (e) Li_xCoO_2 as a function of Li concentration for the various methods considered in this work. The panels are labeled by the transition metal. Experimental values are shown as black horizontal lines [68,73,74,76,77,84–86].

For Li_xCoO_2, we also consider the separate "half-voltages," i.e., the distinct voltage averages for $0 < x < \frac{1}{2}$ and $\frac{1}{2} < x < 1$, shown in Fig. 4 for DFT. In Fig. 4, one can observe the same main trends discussed above for the Li_xCoO_2 V over the full range of x: (1) SCAN significantly increases the voltage, exceeding experiment and (2) incorporating explicit vdW interactions moderately enhances the voltages when added to PBE, but negligibly when added to SCAN. We focus on the "voltage gap" at $x = \frac{1}{2}$, i.e., the difference between the voltage average of $\frac{1}{2} < x < 1$ and that of $0 < x < \frac{1}{2}$. Such a voltage gap ΔV is a measure of the formation energy

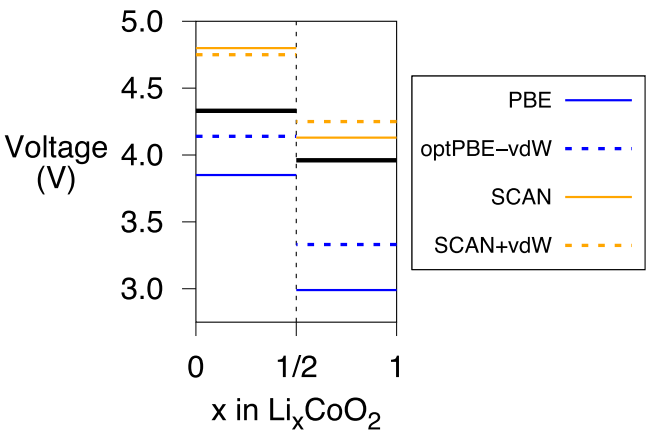

FIG. 4. Average Li_xCoO_2 intercalation voltage for $0 < x < \frac{1}{2}$ (left horizontal lines) and $\frac{1}{2} < x < 1$ (right horizontal lines) within PBE, optPBE-vdW, SCAN, and SCAN+vdW for DFT (i.e., $U = 0$). The solid black horizontal lines indicate the corresponding experimental values.

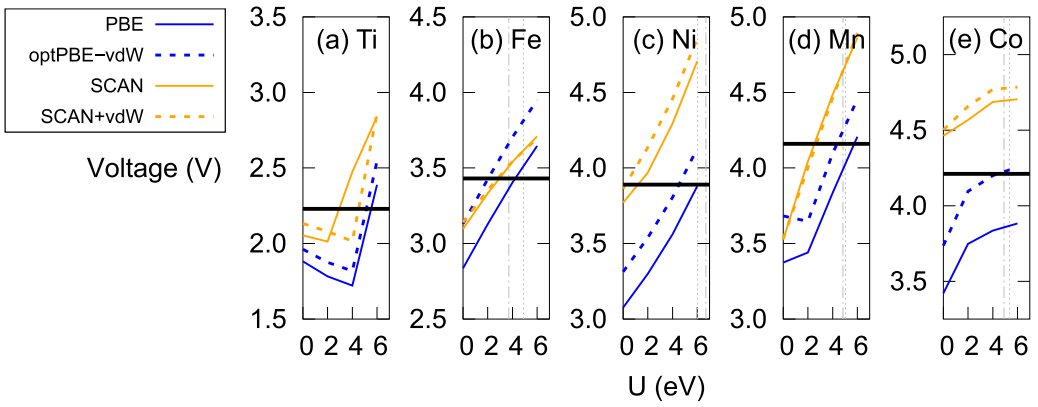

FIG. 5. Average intercalation voltage as a function of U for $0 < x < 1$ within PBE, optPBE-vdW, SCAN, and SCAN+vdW for DFT + U for (a) Li_xTiS_2, (b) Li_xFePO_4, (c) Li_xNiO_2, (d) $Li_xMn_2O_4$, and (e) Li_xCoO_2. The solid black horizontal lines indicate the experimental voltage. First-principles U values from PBE linear response calculations [10,87] are included when available as gray dotted ($x = 0$) and dotted-dashed ($x = 1$) lines.

of a stable (on the convex hull) phase of intermediate Li concentration with respect to the $x = 0$ and 1 end members, which can be written as $-x(1-x)e\Delta V$ [19]. Therefore, the $x = \frac{1}{2}$ voltage gap of Li_xCoO_2 is a convenient benchmark for compositional phase stability. The voltage gap predicted by PBE (−0.9 V) is significantly larger in magnitude than the experimental value (−0.4 V). SCAN predicts an improved, but still too large (in magnitude), voltage gap of −0.7 V. This is consistent with the conclusion that SCAN provides an improved, though still imperfect, description of the energetics of battery cathode materials. vdW interactions also improve the predicted ΔV, yielding values of −0.8 V for optPBE-vdW and −0.5 V for SCAN+vdW.

C. DFT + U

Figure 5 shows the DFT + U average intercalation voltages over the full Li concentration range. We first comment on the general impact of U on the intercalation voltages. Although an increase in V has typically been found with increasing U for battery cathode materials (shown here as well as in previous works [9,10,16,19,21,22]), we also find the opposite behavior in the small-U limit in some of the cases (e.g., Li_xTiS_2). An increase in V with U necessarily stems from the larger energy penalty on the $x = 0$ end member than the $x = 1$ end member, since eV is proportional to $E(0) - E(1)$. Similarly, a decrease in V with U corresponds to a greater energetic penalty on $x = 1$ than $x = 0$.

Nominal electron counting corresponding to completely filled or completely empty states (as suggested by most of the level diagrams in Fig. 1) is insufficient by itself to explain these trends, as the energy penalty from DFT + U (using the FLL double counting) exactly vanishes in such a fully localized limit, as can be seen in Eq. (3). However, knowledge of the electron counting in conjunction with the overall electronic structure can be used to explain the observed trends. For example, for Li_xCoO_2, U penalizes metallic $x = 0$ more than the band insulator $x = 1$, which has closer-to-integer d-orbital occupations [21] due to electron counting (as well as to the increased ionicity stemming from Li). Therefore, V increases with U. The reverse situation occurs for Li_xTiS_2: here, $x = 0$ is the band insulator and $x = 1$ has a partially filled t_{2g} shell, corresponding to a metal. This explains the decrease in V in the small-U limit (the increase at larger U is discussed later). Analogously, a negative $\partial V/\partial U$ in the small-U limit is also found for $Li_xMn_2O_4$ using PBE and optPBE-vdW since within these levels of theory Mn_2O_4 is insulating and $LiMn_2O_4$ is metallic for small U. The voltage increases with U for Li_xFePO_4 and Li_xNiO_2, though the origin of the increases is different than the Li_xCoO_2 case. For Li_xFePO_4, whose end members are both magnetic insulators, it is the enhanced covalency of the $x = 0$ end member [21] that gives it a larger energy penalty. And for Li_xNiO_2, despite the nominally partially filled e_g shell for $x = 1$, the increased ordering from the Jahn-Teller distortion allows the $x = 1$ end member to be less affected by U than the $x = 0$ end member.

Due to the diversity of behavior observed, we now discuss the specific results (including the behavior with different levels of theory in comparison with experiment) for each material separately. Afterward, we present a general synthesis of the results.

We begin with Li_xTiS_2. As discussed above, small values of U for Li_xTiS_2 serve to decrease the predicted V, which already underestimates the experimental value within pure DFT. We also note that, for the majority of the pure DFT levels of theory considered here, U also hurts the volume prediction (shown in Fig. 6) for Li_xTiS_2. Therefore, in the case of Li_xTiS_2, adding Hubbard U serves to hurt the description. Consistent with this finding, we note that the past work of Chevrier *et al.* avoided the use of Hubbard U for Ti-based compounds [14].

Here, we comment on the discontinuous behavior at larger U. A metal-insulator transition for $LiTiS_2$ at larger U decreases its energy penalty relative to TiS_2, leading to a change in sign in $\partial V/\partial U$. The insulating behavior is spurious as $LiTiS_2$ is actually metallic in experiment [88]. This raises the question of whether this predicted insulating state for $LiTiS_2$ for larger U corresponds to (1) an intrinsic failure of DFT + U or simply (2) the use of an unphysically large U parameter. Using a self-consistent linear response approach and PBE, Shishkin and Sato computed U of 5.5 eV for $LiTiS_2$ (using same the PAW potential for Ti we employ, which treats the

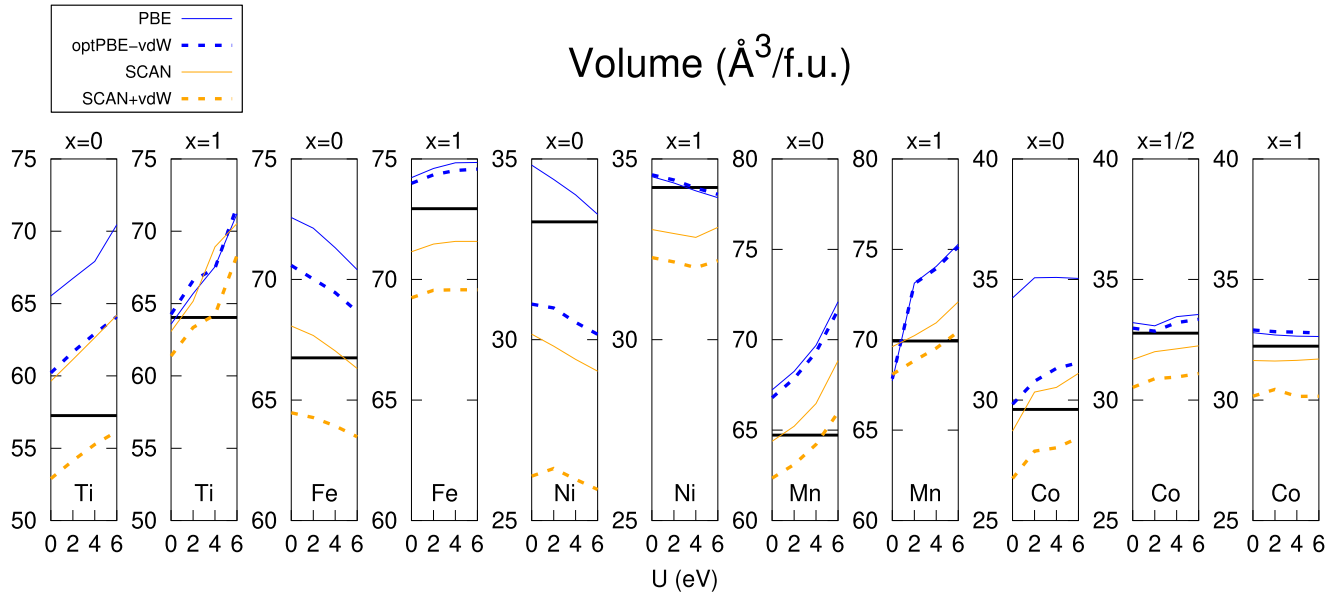

FIG. 6. Volumes in Å^3 per formula unit within DFT + U for Li_xTiS_2, Li_xFePO_4, Li_xNiO_2, $Li_xMn_2O_4$, and Li_xCoO_2 as a function of U for the various methods considered in this work. The panels are labeled by the transition metal and Li concentration. Experimental values are shown as black horizontal lines [68,73,74,76,77,84–86].

4s semicore states as valence states) [20]. Since Shishkin and Sato found $LiTiS_2$ to still be metallic at this U value [20], their results suggest the second case above (too large U); however, we note that this may be a borderline case as we find insulating $LiTiS_2$ for $U = 6$ eV.

In conjunction with the pure DFT results discussed above, we find that the application of SCAN (as opposed to PBE) and vdW interactions significantly improves the voltage prediction for Li_xTiS_2, while U hurts the description. We note that SCAN+vdW, which exhibits the best agreement with the experimental V (error of only 0.1 V), has worse volume predictions than those of SCAN for Li_xTiS_2 (for $LiTiS_2$ in particular), as shown in Fig. 3.

For Li_xFePO_4, the pure DFT approaches are insufficient to quantitatively describe the voltage. However, the predicted voltage increases roughly linearly with U in all cases, enabling agreement with experiment using DFT + U. For PBE, the optimal U value to achieve agreement with experiment is 4.2 V, in agreement with previous work [9,10,21]. This value also agrees well with the overall magnitude of the first-principles U values for the $x = 0$ (4.9 V) and $x = 1$ (3.7 V) end members computed from first principles (with PBE) via the linear response approach [10]. Since adding vdW interactions to PBE (i.e., optPBE-vdW) provides a roughly rigid increase in the predicted V, of around 0.3 V, the optimal U value to achieve agreement with the experimental V for optPBE-vdW is 2.0 eV, substantially lower than the PBE case. SCAN + U and SCAN + vdW + U yield essentially identical V predictions, consistent with the intrinsic vdW interactions in SCAN. For such methods, the predicted V matches experiment for $U = 3.0$ eV, also significantly lower than the PBE case.

Although not computed here, it would be interesting to assess whether the first-principles U values based on optPBE-vdW and/or SCAN(+vdW) would also be appreciably lower than those of PBE, leading to the same consistency observed for PBE in terms of the first-principles U and U fit to experimental V. We note that the optimal $U = 3.0$ eV for SCAN(+vdW), in terms of V, agrees well with U values found to reproduce the FeO/Fe_2O_3 (2.9 eV) and FeO/Fe_3O_4 (3.3 eV) experimental oxidation reaction energies in a recent SCAN + U work by Sai Gautam and Carter [89].

The volume behavior for Li_xFePO_4 is shown in Fig. 6. SCAN + U yields the best volume prediction for Li_xFePO_4 among all the methods considered in this work, though some underestimation of the $LiFePO_4$ volume persists. The band gap and local Fe magnetic moment behaviors for Li_xFePO_4 are shown in the Supplemental Material [83]. The application of U to SCAN also significantly improves the predicted $LiFePO_4$ band gap, though the $FePO_4$ gap (already in good agreement with experiment for $U = 0$) becomes overestimated. A similar effect is found in terms of the local Fe magnetic moment, with overestimation (underestimation) for $FePO_4$ ($LiFePO_4$). Ultimately, while U can be chosen to yield agreement with the experimental V using DFT + U based on any of the pure DFT methodologies considered here, we find that SCAN + U using U of ∼3 eV provides the best (although still imperfect) overall description of Li_xFePO_4 when also taking into account the volume, band gap, and local magnetic moments.

For Li_xNiO_2, the pure DFT prediction using PBE significantly underestimates experiment, but agreement can be reached for U of ∼6 eV, which is close in value to the PBE first-principles computed end member U values [10]. The behavior is similar for optPBE-vdW + U, whose V predictions are ∼0.2 eV larger than those of PBE + U. The behavior for SCAN is quite distinct. Here, the SCAN-predicted V already exhibits excellent agreement (within ∼0.1 V) with experiment even without Hubbard U. Therefore, the application of U in this case pushes V to far too large values. This is also true for SCAN + vdW + U, which exhibits a small, roughly constant ∼0.1 V increase in V with respect to SCAN + U.

Although one can achieve a satisfactory quantitative V prediction using PBE/optPBE-vdW with U (∼6 eV) or SCAN(+vdW) without U, the volume prediction (shown in Fig. 6) suggests such approaches are not equivalent in their overall description. SCAN and SCAN+vdW provide worsened volume predictions as compared to PBE + U. Although optPBE-vdW + U yields a similar $LiNiO_2$ volume as PBE + U, its volume prediction for NiO_2 is significantly worse than PBE + U. We note additionally that PBE + U yields an accurate band-gap prediction for $LiNiO_2$, as shown in the Supplemental Material [83]. Overall, despite the excellent V prediction using SCAN(+vdW), we find PBE + U provides the overall best description of Li_xNiO_2.

The $Li_xMn_2O_4$ case is similar to that of Li_xFePO_4 in that a quantitatively accurate V prediction can be achieved using calculations based on any of the pure DFT methodologies considered here, but only using Hubbard U. U values of 5.7 eV (reasonably close in value to the first-principles computed end member U values [10]) and 4.4 eV are needed to achieve agreement with the experimental V for PBE and optPBE-vdW, respectively. The SCAN + U and SCAN + vdW + U voltages agree with experiment for the significantly smaller value of $U = 2.6$ eV. This value is in good agreement with the U values found to reproduce the MnO/Mn_2O_3 (2.9 eV) and Mn_2O_3/MnO_2 (2.5 eV) experimental oxidation reaction energies in the work of Sai Gautam and Carter [89].

Here, as in the Li_xFePO_4 case, the SCAN+vdW V result is nearly identical to that of SCAN. This suggests that the energetic impact of the vdW interactions in SCAN+vdW beyond those already contained within SCAN itself is especially small for the nonlayered cathode materials. In contrast, optPBE-vdW + U yields a substantially larger V prediction than PBE + U. Based on the volume data shown in Fig. 6 and band-gap data shown in the Supplemental Material [83], we find that DFT + U calculations based on SCAN exhibit a better overall description than those based on PBE for $Li_xMn_2O_4$. In particular, SCAN + U and SCAN + vdW + U do not exhibit the significant volume overestimation of PBE + U and optPBE-vdW + U for appreciable U. In addition, the $LiMn_2O_4$ band gap is underestimated by SCAN + U and SCAN + vdW + U by a much smaller degree than PBE + U and optPBE-vdW + U.

The Li_xCoO_2 voltage is significantly underestimated within pure DFT using PBE (by 0.8 V). The significant increase in the predicted V when adding U to PBE, which is dampened via a spurious metal-insulator transition for CoO_2, is still insufficient to achieve agreement with the experimental V [16,19,21]. As was previously shown [16], adding vdW interactions via optPBE-vdW + U further enhances V with respect to PBE + U and enables agreement with experiment. Therefore, it was suggested [16] that such nonlocal correlation effects were associated with the V underprediction within PBE + U for Li_xCoO_2 (and possibly other transition metal oxides). We reproduce the previous result here and find that the optPBE-vdW + U voltage agrees with experiment for $U = 4.4$ eV.

SCAN provides a drastically different V prediction for Li_xCoO_2 [13,23], moderately *over*estimating (by 0.3 V) the experimental voltage. Since U serves to increase V in this case, the SCAN + U voltage predictions for Li_xCoO_2 become even further from experiment. As observed in many of the cases discussed above, adding vdW interactions to SCAN + U (SCAN + vdW + U) has a relatively modest impact as compared to the difference between optPBE-vdW + U and PBE + U. SCAN + vdW + U provides V predictions for Li_xCoO_2 no more than 0.1 V larger (further from experiment) than SCAN + U.

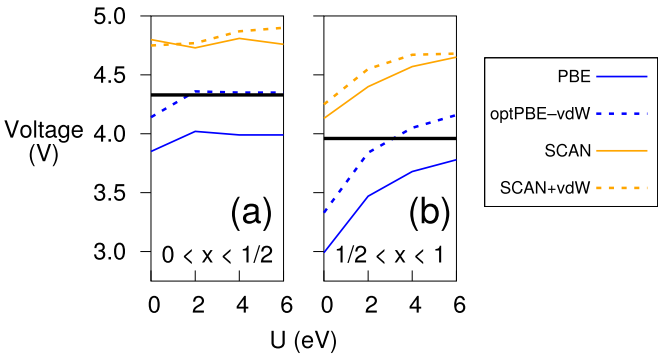

FIG. 7. Li_xCoO_2 intercalation voltage for (a) $x < \frac{1}{2}$ and (b) $x > \frac{1}{2}$ within PBE, optPBE-vdW, SCAN, and SCAN+vdW for DFT + U. The solid black horizontal lines indicate the experimental voltage.

Similar behavior is found in terms of the half-voltages for Li_xCoO_2, shown in Fig. 7: (1) For PBE, U enhances the half-voltages, but not enough to reach experimental values, (2) optPBE-vdW + U provides a substantial increase over PBE + U and enables agreement with experiment (for U close to 3 eV), and (3) U (vdW interactions) generally tends to significantly (moderately) enhance the already-too-large voltages of SCAN. We note that, despite U further overestimating the voltage magnitudes when applied to SCAN(+vdW), it does lead to an improved voltage gap at $x = \frac{1}{2}$.

Although optPBE-vdW + U achieves agreement with the experimental voltage (overall the full and half x ranges), it may not provide an accurate overall description of Li_xCoO_2. As shown in the Supplemental Material [83], although it exhibits an accurate prediction of the $LiCoO_2$ band gap, optPBE-vdW + U exhibits the same spurious orderings as PBE + U: CoO_2 gap opening and large magnetic moment of PBE + U, as well as $Li_{1/2}CoO_2$ charge ordering and gap opening.

We discuss two possible alternatives to optPBE-vdW + U for best describing Li_xCoO_2. The first alternative is to use pure SCAN. Despite modest voltage overestimation (e.g., 0.3 V for $0 < x < 1$), SCAN does not exhibit any of the spurious gap opening or charge ordering discussed above. It also exhibits a very accurate $LiCoO_2$ band gap, $Li_{1/2}CoO_2$ magnetic moment, and reasonably accurate volume predictions, as shown in Fig. 3 and the Supplemental Material [83]. In addition, although the overall voltage magnitudes are moderately overestimated, the $x = \frac{1}{2}$ voltage gap (related to the $x = \frac{1}{2}$ formation energy) agrees decently well with experiment, as discussed in the previous section. The second alternative is to use DFT+DMFT (to which DFT + U is a static approximation ignoring dynamical correlations) in conjunction with SCAN, as very recent work using non-charge-self-consistent DFT+DMFT [23] found that dynamical correlations (1) are large and x dependent in Li_xCoO_2, (2) help eliminate the

spurious gaps and charge ordering of DFT + U, and (3) reduce the predicted V such that the SCAN+DMFT voltage is likely to agree well with experiment. Further work to assess which of these alternatives (or another) is optimal to accurately describe Li_xCoO_2 will be important future work.

Finally, we summarize our overall findings regarding describing battery cathode materials within DFT + U. As discussed in the previous section, within pure DFT, it is clear that (1) SCAN is superior to PBE and (2) adding additional vdW interactions beyond those intrinsic to SCAN is not essential and is in some cases detrimental. With DFT + U, the results are less clear cut.

In the case of Li_xTiS_2, adding Hubbard U generally yields no improvement over the corresponding pure DFT V results (which are only modestly underestimated with SCAN and SCAN+vdW), if one takes into account the spurious $LiTiS_2$ metal-insulator transition predicted by DFT + U occurring for sufficiently large U. In contrast, Hubbard U is essential to achieve a voltage prediction in agreement with experiment for Li_xFePO_4 and $LiMn_2O_4$. Therefore, the new SCAN functional does not eliminate the need for Hubbard-U corrections. In fact, we find SCAN + U provides the best description of these two cathode materials. Therefore, it is not true that SCAN eliminates the need for U for battery cathode materials in general, which Chakraborty *et al.* found to be the case for several layered oxide cathodes [13]. Although SCAN provides an excellent voltage prediction for Li_xNiO_2, an improved description can be achieved via DFT + U calculations based on PBE. Therefore, we find that calculations based on SCAN should not be universally considered superior to those based on PBE. Finally, in the case of Li_xCoO_2, none of the methods considered here give a sufficient description of both the voltage and electronic structure, though SCAN arguably fares the best.

Taking all these results into account, despite the improved performance obtained via pure DFT and DFT + U calculations based on SCAN for certain cases, we find that no single method can sufficiently accurately describe the voltage and overall structural, electronic, and magnetic properties (i.e., yielding errors no more than 5% for voltage, volume, band gap, and magnetic moments) of the battery cathode materials considered here. Our results strongly motivate the need for improved electronic structure approaches for such systems.

V. CONCLUSIONS

Despite the great need for an accurate and computationally inexpensive approach to characterize and design battery cathode materials, such a method still remains out of reach at present. Within pure DFT, SCAN is a significant improvement over PBE for describing cathode materials, though appreciable errors remain. Methods incorporating explicit vdW interactions are not critical and in cases even detrimental when applied in conjunction with SCAN, which already intrinsically contains some intermediate-range vdW interactions.

Hubbard-U corrections considered within DFT + U are essential to achieve an accurate voltage prediction in some cases (e.g., Li_xFePO_4 and $Li_xMn_2O_4$) and detrimental in others (e.g., Li_xTiS_2). Although we find SCAN + U provides the best description for Li_xFePO_4 and $Li_xMn_2O_4$, we find PBE + U gives the best description for Li_xNiO_2, suggesting DFT + U calculations based on SCAN should not be considered universally superior to those based on PBE. No method here is completely satisfactory to describe Li_xCoO_2, though the SCAN description perhaps has the fewest deficiencies. Overall, a "one size fits all" method unfortunately does not currently exist for battery cathode materials. Our results motivate the need to develop improved electronic structure descriptions that can accurately describe the thermodynamics and electronic structure of this important class of materials.

ACKNOWLEDGMENTS

We acknowledge support from Toyota Research Institute through the Accelerated Materials Design and Discovery program (development of software tools for automating electronic structure calculations) and the Center for Electrochemical Energy Science (CEES), an Energy Frontier Research Center funded by the US Department of Energy, Office of the Science, Basic Energy Science under Award No. DE-AC02-06CH11357 (voltage calculations). Computational resources were provided by the National Energy Research Scientific Computing Center (US Department of Energy Contract No. DE-AC02-05CH11231) and the Extreme Science and Engineering Discovery Environment (National Science Foundation Contract No. ACI-1548562).

[1] M. K. Aydinol, A. F. Kohan, G. Ceder, K. Cho, and J. Joannopoulos, Phys. Rev. B **56**, 1354 (1997).
[2] C. Wolverton and A. Zunger, Phys. Rev. B **57**, 2242 (1998).
[3] Y. Reynier, J. Graetz, T. Swan-Wood, P. Rez, R. Yazami, and B. Fultz, Phys. Rev. B **70**, 174304 (2004).
[4] P. Hohenberg and W. Kohn, Phys. Rev. **136**, B864 (1964).
[5] W. Kohn and L. J. Sham, Phys. Rev. **140**, A1133 (1965).
[6] J. P. Perdew, K. Burke, and M. Ernzerhof, Phys. Rev. Lett. **77**, 3865 (1996).
[7] A. K. Padhi, K. S. Nanjundaswamy, and J. B. Goodenough, J. Electrochem. Soc. **144**, 1188 (1997).
[8] A. K. Padhi, K. S. Nanjundaswamy, and J. B. Goodenough, J. Electrochem. Soc. **144**, 1609 (1997).
[9] F. Zhou, C. A. Marianetti, M. Cococcioni, D. Morgan, and G. Ceder, Phys. Rev. B **69**, 201101(R) (2004).
[10] F. Zhou, M. Cococcioni, C. A. Marianetti, D. Morgan, and G. Ceder, Phys. Rev. B **70**, 235121 (2004).
[11] C. Wolverton and A. Zunger, Phys. Rev. Lett. **81**, 606 (1998).
[12] B. Wang, S. Luo, and D. G. Truhlar, J. Phys. Chem. B **120**, 1437 (2016).
[13] A. Chakraborty, M. Dixit, D. Aurbach, and D. T. Major, npj Comput. Mater. **4**, 60 (2018).
[14] V. L. Chevrier, S. P. Ong, R. Armiento, M. K. Y. Chan, and G. Ceder, Phys. Rev. B **82**, 075122 (2010).
[15] D.-H. Seo, A. Urban, and G. Ceder, Phys. Rev. B **92**, 115118 (2015).

[16] M. Aykol, S. Kim, and C. Wolverton, J. Phys. Chem. C **119**, 19053 (2015).

[17] O. Le Bacq, A. Pasturel, and O. Bengone, Phys. Rev. B **69**, 245107 (2004).

[18] S. P. Ong, V. L. Chevrier, G. Hautier, A. Jain, C. Moore, S. Kim, X. Ma, and G. Ceder, Energy Environ. Sci. **4**, 3680 (2011).

[19] M. Aykol and C. Wolverton, Phys. Rev. B **90**, 115105 (2014).

[20] M. Shishkin and H. Sato, Phys. Rev. B **93**, 085135 (2016).

[21] E. B. Isaacs and C. A. Marianetti, Phys. Rev. B **95**, 045141 (2017).

[22] M. Cococcioni and N. Marzari, Phys. Rev. Mater. **3**, 033801 (2019).

[23] E. B. Isaacs and C. A. Marianetti, arXiv:1903.10436.

[24] K. Saritas, E. R. Fadel, B. Kozinsky, and J. C. Grossman, J. Phys. Chem. C **124**, 5893 (2020).

[25] R. M. Martin, *Electronic Structure: Basic Theory and Practical Methods* (Cambridge University Press, New York, 2008).

[26] D. M. Ceperley and B. J. Alder, Phys. Rev. Lett. **45**, 566 (1980).

[27] J. Sun, A. Ruzsinszky, and J. P. Perdew, Phys. Rev. Lett. **115**, 036402 (2015).

[28] J. Sun, R. C. Remsing, Y. Zhang, Z. Sun, A. Ruzsinszky, H. Peng, Z. Yang, A. Paul, U. Waghmare, X. Wu, M. L. Klein, and J. P. Perdew, Nat. Chem. **8**, 831 (2016).

[29] F. Tran, J. Stelzl, and P. Blaha, J. Chem. Phys. **144**, 204120 (2016).

[30] D. A. Kitchaev, H. Peng, Y. Liu, J. Sun, J. P. Perdew, and G. Ceder, Phys. Rev. B **93**, 045132 (2016).

[31] Y. Zhang, J. Sun, J. P. Perdew, and X. Wu, Phys. Rev. B **96**, 035143 (2017).

[32] H. Peng, Z.-H. Yang, J. P. Perdew, and J. Sun, Phys. Rev. X **6**, 041005 (2016).

[33] C. Lane, J. W. Furness, I. G. Buda, Y. Zhang, R. S. Markiewicz, B. Barbiellini, J. Sun, and A. Bansil, Phys. Rev. B **98**, 125140 (2018).

[34] Y. Yao and Y. Kanai, J. Chem. Phys. **146**, 224105 (2017).

[35] A. P. Bartók and J. R. Yates, J. Chem. Phys. **150**, 161101 (2019).

[36] J. W. Furness and J. Sun, Phys. Rev. B **99**, 041119(R) (2019).

[37] E. B. Isaacs and C. Wolverton, Phys. Rev. Mater. **2**, 063801 (2018).

[38] Y. Zhang, D. A. Kitchaev, J. Yang, T. Chen, S. T. Dacek, R. A. Sarmiento-Pérez, M. A. L. Marques, H. Peng, G. Ceder, J. P. Perdew, and J. Sun, npj Comput. Mater. **4**, 9 (2018).

[39] S. Grimme, Wiley Interdiscip. Rev.: Comput. Mol. Sci. **1**, 211 (2011).

[40] J. Klimeš and A. Michaelides, J. Chem. Phys. **137**, 120901 (2012).

[41] K. Berland, V. R. Cooper, K. Lee, E. Schröder, T. Thonhauser, P. Hyldgaard, and B. I. Lundqvist, Rep. Prog. Phys. **78**, 066501 (2015).

[42] S. Grimme, A. Hansen, J. G. Brandenburg, and C. Bannwarth, Chem. Rev. **116**, 5105 (2016).

[43] J. Hermann, R. A. DiStasio, and A. Tkatchenko, Chem. Rev. **117**, 4714 (2017).

[44] M. Stöhr, T. V. Voorhis, and A. Tkatchenko, Chem. Soc. Rev. **48**, 4118 (2019).

[45] M. Dion, H. Rydberg, E. Schröder, D. C. Langreth, and B. I. Lundqvist, Phys. Rev. Lett. **92**, 246401 (2004).

[46] G. Román-Pérez and J. M. Soler, Phys. Rev. Lett. **103**, 096102 (2009).

[47] J. Klimeš, D. R. Bowler, and A. Michaelides, J. Phys.: Condens. Matter **22**, 022201 (2010).

[48] J. Klimeš, D. R. Bowler, and A. Michaelides, Phys. Rev. B **83**, 195131 (2011).

[49] B. Hammer, L. B. Hansen, and J. K. Nørskov, Phys. Rev. B **59**, 7413 (1999).

[50] P. Jurečka, J. Šponer, J. Černý, and P. Hobza, Phys. Chem. Chem. Phys. **8**, 1985 (2006).

[51] O. A. Vydrov and T. Van Voorhis, J. Chem. Phys. **133**, 244103 (2010).

[52] R. Sabatini, T. Gorni, and S. de Gironcoli, Phys. Rev. B **87**, 041108(R) (2013).

[53] B. Himmetoglu, A. Floris, S. de Gironcoli, and M. Cococcioni, Int. J. Quantum Chem. **114**, 14 (2014).

[54] S. L. Dudarev, G. A. Botton, S. Y. Savrasov, C. J. Humphreys, and A. P. Sutton, Phys. Rev. B **57**, 1505 (1998).

[55] V. I. Anisimov, I. V. Solovyev, M. A. Korotin, M. T. Czyżyk, and G. A. Sawatzky, Phys. Rev. B **48**, 16929 (1993).

[56] P. E. Blöchl, Phys. Rev. B **50**, 17953 (1994).

[57] G. Kresse and D. Joubert, Phys. Rev. B **59**, 1758 (1999).

[58] G. Kresse and J. Hafner, Phys. Rev. B **49**, 14251 (1994).

[59] G. Kresse and J. Hafner, Phys. Rev. B **47**, 558 (1993).

[60] G. Kresse and J. Furthmüller, Phys. Rev. B **54**, 11169 (1996).

[61] G. Kresse and J. Furthmüller, Comput. Mater. Sci. **6**, 15 (1996).

[62] A. I. Liechtenstein, V. I. Anisimov, and J. Zaanen, Phys. Rev. B **52**, R5467 (1995).

[63] Recommended PAW potentials for DFT calculations using vasp.5.2, https://cms.mpi.univie.ac.at/vasp/vasp/Recommended_PAW_potentials_DFT_calculations_using_vasp_5_2.html.

[64] M. Methfessel and A. T. Paxton, Phys. Rev. B **40**, 3616 (1989).

[65] P. E. Blöchl, O. Jepsen, and O. K. Andersen, Phys. Rev. B **49**, 16223 (1994).

[66] R. R. Chianelli, J. C. Scanlon, and A. H. Thompson, Mater. Res. Bull. **10**, 1379 (1975).

[67] J. R. Dahn, W. R. McKinnon, R. R. Haering, W. J. L. Buyers, and B. M. Powell, Can. J. Phys. **58**, 207 (1980).

[68] G. G. Amatucci, J. M. Tarascon, and L. C. Klein, J. Electrochem. Soc. **143**, 1114 (1996).

[69] W. D. Johnston, R. R. Heikes, and D. Sestrich, J. Phys. Chem. Solids **7**, 1 (1958).

[70] H. J. Orman and P. J. Wiseman, Acta Crystallogr. Sect. C **40**, 12 (1984).

[71] L. Seguin, G. Amatucci, M. Anne, Y. Chabre, P. Strobel, J. M. Tarascon, and G. Vaughan, J. Power Sources **81-82**, 604 (1999).

[72] L. Croguennec, C. Pouillerie, and C. Delmas, J. Electrochem. Soc. **147**, 1314 (2000).

[73] J. Cao, H. Zou, C. Guo, Z. Chen, and S. Pu, Solid State Ionics **180**, 1209 (2009).

[74] Y. Takahashi, N. Kijima, K. Tokiwa, T. Watanabe, and J. Akimoto, J. Phys.: Condens. Matter **19**, 436202 (2007).

[75] R. P. Santoro and R. E. Newnham, Acta Crystallogr. **22**, 344 (1967).

[76] G. Rousse, J. Rodriguez-Carvajal, S. Patoux, and C. Masquelier, Chem. Mater. **15**, 4082 (2003).

[77] J. C. Hunter, J. Solid State Chem. **39**, 142 (1981).

[78] A. Mosbah, A. Verbaere, and M. Tournoux, Mater. Res. Bull. **18**, 1375 (1983).
[79] S. Kim, M. Aykol, and C. Wolverton, Phys. Rev. B **92**, 115411 (2015).
[80] M. S. Whittingham, Science **192**, 1126 (1976).
[81] C. Delmas, M. Ménétrier, L. Croguennec, S. Levasseur, J. P. Pérès, C. Pouillerie, G. Prado, L. Fournès, and F. Weill, Int. J. Inorg. Mater. **1**, 11 (1999).
[82] J. Barker, K. West, Y. Saidi, R. Pynenburg, B. Zachau-Christiansen, and R. Koksbang, J. Power Sources **54**, 475 (1995).
[83] See Supplemental Material at http://link.aps.org/supplemental/10.1103/PhysRevMaterials.4.065405 for additional calculation results (magnetic moment, band gap, and density of states) and details on the experimental voltage data [90–112].
[84] M. S. Whittingham and F. R. Gamble, Mater. Res. Bull. **10**, 363 (1975).
[85] K. Mizushima, P. Jones, P. Wiseman, and J. Goodenough, Mater. Res. Bull. **15**, 783 (1980).
[86] A. Hirano, R. Kanno, Y. Kawamoto, Y. Takeda, K. Yamaura, M. Takano, K. Ohyama, M. Ohashi, and Y. Yamaguchi, Solid State Ionics **78**, 123 (1995).
[87] M. Cococcioni and S. de Gironcoli, Phys. Rev. B **71**, 035105 (2005).
[88] P. C. Klipstein and R. H. Friend, J. Phys. C: Solid State Phys. **20**, 4169 (1987).
[89] G. Sai Gautam and E. A. Carter, Phys. Rev. Mater. **2**, 095401 (2018).
[90] J. E. Greedan, N. P. Raju, A. S. Wills, C. Morin, S. M. Shaw, and J. N. Reimers, Chem. Mater. **10**, 3058 (1998).
[91] K. Mukai and J. Sugiyama, Chem. Lett. **38**, 944 (2009).
[92] T. Motohashi, T. Ono, Y. Sugimoto, Y. Masubuchi, S. Kikkawa, R. Kanno, M. Karppinen, and H. Yamauchi, Phys. Rev. B **80**, 165114 (2009).
[93] J. van Elp, J. L. Wieland, H. Eskes, P. Kuiper, G. A. Sawatzky, F. M. F. de Groot, and T. S. Turner, Phys. Rev. B **44**, 6090 (1991).
[94] J. Molenda, P. Wilk, and J. Marzec, Solid State Ionics **146**, 73 (2002).
[95] F. Zhou, K. Kang, T. Maxisch, G. Ceder, and D. Morgan, Solid State Commun. **132**, 181 (2004).
[96] K. Zaghib, A. Mauger, J. B. Goodenough, F. Gendron, and C. M. Julien, Chem. Mater. **19**, 3740 (2007).
[97] C. de Vaulx, M.-H. Julien, C. Berthier, S. Hébert, V. Pralong, and A. Maignan, Phys. Rev. Lett. **98**, 246402 (2007).
[98] T. Motohashi, Y. Katsumata, T. Ono, R. Kanno, M. Karppinen, and H. Yamauchi, Chem. Mater. **19**, 5063 (2007).
[99] S. Kawasaki, T. Motohashi, K. Shimada, T. Ono, R. Kanno, M. Karppinen, H. Yamauchi, and G.-q. Zheng, Phys. Rev. B **79**, 220514(R) (2009).
[100] K. Miyoshi, C. Iwai, H. Kondo, M. Miura, S. Nishigori, and J. Takeuchi, Phys. Rev. B **82**, 075113 (2010).
[101] T. Y. Ou-Yang, F.-T. Huang, G. J. Shu, W. L. Lee, M.-W. Chu, H. L. Liu, and F. C. Chou, Phys. Rev. B **85**, 035120 (2012).
[102] K. Kushida and K. Kuriyama, Appl. Phys. Lett. **77**, 4154 (2000).
[103] C. Ouyang, H. Deng, Z. Ye, M. Lei, and L. Chen, Thin Solid Films **503**, 268 (2006).
[104] M. W. Raja, S. Mahanty, P. Ghosh, R. N. Basu, and H. S. Maiti, Mater. Res. Bull. **42**, 1499 (2007).
[105] S. Douafer, H. Lahmar, M. Benamira, G. Rekhila, and M. Trari, J. Phys. Chem. Solids **118**, 62 (2018).
[106] J. N. Reimers and J. R. Dahn, J. Electrochem. Soc. **139**, 2091 (1992).
[107] T. Ohzuku and A. Ueda, J. Electrochem. Soc. **141**, 2972 (1994).
[108] A. Yamada, S. C. Chung, and K. Hinokuma, J. Electrochem. Soc. **148**, A224 (2001).
[109] D. Y. W. Yu, C. Fietzek, W. Weydanz, K. Donoue, T. Inoue, H. Kurokawa, and S. Fujitani, J. Electrochem. Soc. **154**, A253 (2007).
[110] S. Yamada, M. Fujiwara, and M. Kanda, J. Power Sources **54**, 209 (1995).
[111] H. Arai, S. Okada, Y. Sakurai, and J.-i. Yamaki, Solid State Ionics **95**, 275 (1997).
[112] J. R. Dahn and R. R. Haering, Solid State Commun. **40**, 245 (1981).